

ORIGINAL ARTICLE

Kinetic analysis of drug–target interactions with PET for characterization of pharmacological hysteresis

Cristian Salinas¹, David Weinzimmer², Graham Searle¹, David Labaree², Jim Ropchan², Yiyun Huang², Eugenii A Rabiner^{1,3}, Richard E Carson² and Roger N Gunn^{1,3,4}

In vivo characterization of the brain pharmacokinetics of novel compounds provides important information for drug development decisions involving dose selection and the determination of administration regimes. In this context, the compound–target affinity is the key parameter to be estimated. However, if compounds exhibit a dynamic lag between plasma and target bound concentrations leading to pharmacological hysteresis, care needs to be taken to ensure the appropriate modeling approach is used so that the system is characterized correctly and that the resultant estimates of affinity are correct. This work focuses on characterizing different pharmacokinetic models that relate the plasma concentration to positron emission tomography outcomes measurements (e.g., volume of distribution and target occupancy) and their performance in estimating the true *in vivo* affinity. Measured (histamine H₃ receptor antagonist—GSK189254) and simulated data sets enabled the investigation of different modeling approaches. An indirect pharmacokinetic–receptor occupancy model was identified as a suitable model for the calculation of affinity when a compound exhibits pharmacological hysteresis.

Journal of Cerebral Blood Flow & Metabolism (2013) **33**, 700–707; doi:10.1038/jcbfm.2012.208; published online 6 February 2013

Keywords: affinity; GSK189254; histamine H₃; PET; pharmacokinetic model; pharmacological hysteresis

INTRODUCTION

In vivo characterization of the brain pharmacokinetics of novel CNS compounds provides important information for drug development, enabling dose selection and determination of optimal administration regimes. Although *in vitro* estimates of affinity are usually the starting point for pharmacokinetic characterization, *in vivo* conditions such as the presence of endogenous ligands, local ionic environments, receptor clustering, and ligand rebinding effects are difficult to reproduce *in vitro* leading to uncertainty around these estimates. Furthermore, affinity captures only an equilibrium property of the compound and thus it is just one component of a more comprehensive pharmacokinetic characterization. In particular, compounds with slow tissue kinetics relative to plasma, where the drug–target interaction is the rate-limiting process, are characterized by pharmacological hysteresis.¹ Hysteresis is the dependence of a system not only on its current environment but also on its past environment and thus to predict its future development, either its internal state or its history must be known. While hysteresis traditionally concerns systems with alternately increasing and decreasing inputs, where the outputs form a loop, it can also occur in systems where there is a dynamic lag between the input and output. This effect is also referred to as hysteresis, or rate-dependent hysteresis and is the phenomenon studied here in relation to dynamic lags between the plasma and target bound concentrations.

Positron emission tomography (PET) has been used to study the *in vivo* pharmacokinetic properties of ligands binding to receptors in the brain via a number of different methods.² For example multiple injection (MI) protocols using different specific activities (SA) were first proposed by Delforge *et al*³ and subsequently used

to estimate the affinity of labeled compounds, for example, CFT,⁴ fallypride,⁵ and fluorocarazolol.⁶ Further, if a reference region devoid of specific target sites exists, the pseudoequilibrium method or multiple ligand concentration receptor assay can be applied using different SA injections, allowing for estimation of the affinity in an analogous manner to the *in vitro* Scatchard approach.^{7,8} These methods work by achieving different levels of target occupancy via homologous competition with the radiolabeled compound, allowing separate estimates of target density and radioligand affinity. However, during drug development a radiolabeled version of the drug candidate may not exist rendering these methods unviable. An alternate approach involving heterologous competition can be applied if a suitable PET radioligand exists for the target. These methods involve modeling changes in the specific PET outcome measures (V_T , BP_{ND} or target occupancy) due to heterologous competition with the unlabeled compound of interest. Two general models that relate the target occupancy to the plasma concentration can be formulated. The first and simplest model assumes that the target bound concentration of the compound is in equilibrium with the plasma concentration at all times leading to an E_{max} type relationship.⁹ The second approach relates the two quantities in the nonequilibrium condition when a dynamic lag exists between the plasma and target bound concentrations.^{10–12}

In this paper, the *in vivo* affinity of GSK189254, a highly selective histamine H₃ ligand,¹³ was investigated using different analytical methods applied to a nonhuman primate PET study using [¹¹C]GSK189254 as the radioligand. In addition, computer simulations were used to explore a wide range of kinetic behavior that included scenarios where compounds rapidly equilibrated

¹GlaxoSmithKline, Clinical Imaging Centre, Hammersmith Hospital, London, UK; ²Yale PET Center, Yale School of Medicine, New Haven, Connecticut, USA; ³Department of Medicine, Imperial College London, London, UK and ⁴Department of Engineering Science, University of Oxford, Oxford, UK. Correspondence: Professor RN Gunn, Imanova, Centre for Imaging Sciences, Burlington Danes Building, Imperial College London, Hammersmith Hospital, Du Cane Road, London W12 0NN, UK.

E-mail: roger.gunn@imanova.co.uk

Received 16 June 2012; revised 31 October 2012; accepted 28 November 2012; published online 6 February 2013

between plasma and tissue through to scenarios involving a substantial dynamic lag between plasma and target bound concentrations congruous with pharmacological hysteresis. We hypothesized that the different approaches would all provide good estimates of the *in vivo* affinity for compounds that rapidly equilibrate between plasma and tissue but that biased estimates would be obtained for approaches that do not properly account for a dynamic lag between plasma and target bound concentrations in conditions of pharmacological hysteresis.

Theory

This section outlines the mathematical framework for the different methods that estimate affinity.

Multiple injection method. While tracer alone PET studies only allow for the estimation of the product of the available receptor density and affinity (the binding potential), the MI method³ enables estimation of both the available receptor density (B_{avail}) and the radiotracer equilibrium dissociation rate constant (K_d —inversely proportional to affinity). The MI method achieves this by driving the receptor system to different levels of occupancy through the coinjection of cold ligand (i.e., the experiment is performed at different SA). In brief, a set of $2n$ differential equations ($i=1,2, \dots n$ —one for each injection) representing the rate of change of free plus nonspecifically bound (C_{ND}) and specifically bound (C_S) mass concentrations is solved simultaneously to determine K_1 , k_2 , f_{ND} , k_{on} , k_{off} , and B_{avail} .¹⁴

$$\frac{dC_{ND}^i}{dt} = K_1 C_p^i - k_2 C_{ND}^i - f_{ND} k_{on} C_{ND}^i \left(B_{avail} - \sum_j C_S^j \right) + k_{off} C_S^i \quad (1)$$

$$\frac{dC_S^i}{dt} = f_{ND} k_{on} C_{ND}^i \left(B_{avail} - \sum_j C_S^j \right) - k_{off} C_S^i \quad (2)$$

where K_1 and k_2 in $\text{mL} \cdot \text{cm}^{-3} \cdot \text{min}^{-1}$ and min^{-1} , respectively, are the rate constants describing the transit of the ligand between plasma and tissue, k_{on} and k_{off} in min^{-1} are the rate constants describing the target binding, f_{ND} is the free fraction in tissue and B_{avail} is the available target density in nmol/L . C_p^i is the mass input function for injection i in nmol/L .⁴

The apparent equilibrium dissociation rate constant (K_d^{app}) of the compound is defined by the ratio $\frac{k_{off}}{f_{ND} k_{on}}$. The term ‘apparent’ is introduced to reflect the fact that the K_d is measured with respect to the total ligand concentration in tissue rather than the free concentration and furthermore to acknowledge that competing endogenous ligands would also impact this parameter.

The application of the MI method is restricted to homologous competition studies in which both the labeled and unlabeled compounds have the same kinetic properties.

PseudoEquilibrium method. When the bound compartment is in equilibrium with the free compartment (i.e., $\frac{dC_S(t)}{dt} = 0$) equation 2 can be rearranged to derive the relationship $\frac{C_S}{C_{ND}} = \frac{B_{avail} - C_S}{K_d^{app}}$. Under the assumption that a reference region time–activity curve (TAC) can be derived and that its time course is identical to that of the nondisplaceable TAC in a target region, it can be subtracted from the target region TAC to derive an estimate of the bound concentration time course ($C_S(t)$). A pseudo-equilibrium bound concentration can then be determined at the time of the transient equilibrium when $\frac{dC_S(t)}{dt} = 0$. In addition, C_{ND} can be estimated at this time point from the reference TAC, although the lack of correction for tissue nonspecific binding at this point will again leave us using the term ‘apparent’ in the K_d . Acquisition of $\frac{C_S}{C_{ND}}$ and C_S values from multiple scans using different SA injections allows

for the application of a Scatchard plot to derive K_d^{app} as the negative inverse of the slope.⁷ As with the MI approach, the pseudo-equilibrium method is restricted to homologous competition studies.

Direct PK-RO model. A direct pharmacokinetic-receptor occupancy (PK-RO) model can be applied to both homologous and heterologous competition studies. When the kinetics of the unlabeled compound of interest are sufficiently rapid such that its plasma, free tissue, and bound concentrations do not demonstrate any dynamic lag they can be considered in equilibrium at all times. Under these conditions, the relationship between the target occupancy (Occ) and the plasma concentration of the unlabeled compound of interest can be described by

$$Occ = \frac{C_p}{C_p + K_d^{app}} \quad (3)$$

under the assumption full target occupancy can be achieved ($Occ_{max} = 1$) and that there is single site competitive binding. This allows for the estimation of K_d^{app} from occupancy data or alternatively it may be obtained directly from the corresponding equations for BP_{ND} or V_T

$$BP_{ND}^{Block} = BP_{ND}^{Baseline} \left(1 - \frac{C_p}{C_p + K_d^{app}} \right) \quad (4)$$

$$V_T^{Block} = V_{ND} \left(1 + BP_{ND}^{Baseline} \left(1 - \frac{C_p}{C_p + K_d^{app}} \right) \right) \quad (5)$$

where $BP_{ND}^{Baseline}$ is the baseline binding potential and V_{ND} the nondisplaceable volume of distribution of the radioligand. In equations 3, 4, and 5, K_d^{app} may also be denoted by EC_{50} (the plasma concentration required to achieve 50% occupancy).

Indirect PK-RO model. Compounds with a dynamic lag between plasma and target bound concentrations exhibit pharmacological hysteresis and require a more comprehensive model that properly accounts for this lag.^{11,12} In this case the model is said to be indirect. An indirect PK-RO model can be applied to homologous and heterologous competition studies. Such indirect models have been considered previously in the literature^{10,15} and can describe the observed time occupancy curve (TOC(t): fractional occupancy at time t) as a function of the drug concentration by

$$\frac{dTOC(t)}{dt} = k_{on}^{app} C_p(t)(1 - TOC(t)) - k_{off}^{app} TOC(t) \quad (6)$$

This particular model assumes that the rate-limiting step is the interaction between the compound and the target while the transport of the compound between plasma and the target site (e.g., the extracellular space) is sufficiently fast so as to be considered in equilibrium at all times. As K_d^{app} is one of the key parameters of interest, equation 6 was reparameterized in terms of k_{off}^{app} and K_d^{app} and equation 7 was used for all analyses in this work.

$$\frac{dTOC(t)}{dt} = \frac{k_{off}^{app}}{K_d^{app}} (C_p(t)(1 - TOC(t)) - K_d^{app} TOC(t)) \quad (7)$$

For all four of the methods, an apparent dissociation equilibrium constant K_d^{app} is estimated, which differs from the true dissociation equilibrium constant K_d by a factor related to the nonspecific binding in plasma or tissue. In the MI method, the estimation is with respect to the free concentration in tissue, therefore the tissue-free fraction is needed for correction, $K_d = f_{ND} K_d^{app}$. In the other methods, the estimation of the equilibrium dissociation constant is performed with respect to

the plasma concentration and the plasma-free fraction is used to determine the true $K_d (=f_p K_d^{app})$.

MATERIALS AND METHODS

Study Design

^{11}C GSK189254 PET scans were carried out in one adult female baboon (Papio Anubis, ~15 kg) at the Yale PET Center following Institutional Animal Care and Use Committee (IACUC) approval. On each scanning day, the fasted baboon was immobilized with ketamine (10 mg/kg i.m.), glycopyrrolate (0.005 to 0.01 mg/kg i.m.) and anesthetized with 1.5% to 2.5% isoflurane via an endotracheal tube. Vital signs were monitored every 15 minutes and the temperature was kept constant at ~37 °C with heated water blankets. An i.v. catheter was inserted for administration of fluids, drugs, and the PET radiotracer ^{11}C GSK189254 and an arterial catheter was inserted for blood sampling. Nine scans were acquired in total over five scanning sessions performed on separate days. At least 7 days were allowed between each of the scanning sessions for animal recovery and drug clearance. Sessions 1, 2, and 3 consisted of a baseline scan (tracer administration of ^{11}C GSK189254) followed by a nontracer scan at high (session 2), medium (session 1), and low (session 3) SA. The time between the end of the baseline scan and the beginning of the nontracer scan for sessions 1, 2, and 3 was 2.7, 0.8, and 1.7 hours, respectively. For session 4, 1.5 μg /kg of unlabeled GSK189254 was administered i.v. and followed by two tracer scans starting at 1 and 6 hours postadministration. For session 5, 1.5 μg /kg of unlabeled GSK189254 was administered i.v. and followed by a tracer scan at 15 hours.

Using estimates of the GSK189254 affinity obtained previously in humans,¹⁶ the coadministered unlabeled dose was initially selected for scan 2 in session 1 so as to achieve a target occupancy of ~50% in the baboon (0.08 μg /kg). Occupancy estimates from session 1 were then used to adjust the concentration of unlabeled GSK189254 on the subsequent scanning sessions to achieve low (0.035 μg /kg) or high (0.37 μg /kg) levels of target occupancy.

Radiochemistry

Production of ^{11}C CO₂ was initiated with the $^{14}\text{N}(p,\alpha)^{11}\text{C}$ nuclear reaction by bombarding, with a proton source, a mixture of nitrogen with oxygen (0.5% to 1%) in a high pressure target using the GE PETtrace cyclotron. The target was routinely irradiated with a proton beam current of 55 μA for 30 minutes and provided about 111 GBq of ^{11}C CO₂ at the end of bombardment.

The ^{11}C CO₂ was then transferred into a GE MicroLab methyl iodide production module or a GE TRACERLab Fx-C-Pro module installed inside a hot cell and trapped in a mixture of nickel with a molecular sieve. Hydrogen was then passed through the catalyst and reacted with ^{11}C CO₂ to afford ^{11}C CH₄, which was converted to ^{11}C Mel by reaction with iodine at high temperature (720 °C). Radiolabeling was performed in a Bioscan AutoLoop by trapping ^{11}C Mel in a stainless steel tubing loop containing a solution of desmethyl GSK189254 (0.3 to 0.5 mg) and 1 mol/L KOH (2 to 4 μL) in DMF (0.1 mL) and then reacted at ambient temperature for 5 minutes. Radiochemical yield was 6.1% \pm 1.5% (decay-uncorrected, based on ^{11}C Mel), with SA 477 \pm 204 GBq/ μmol at end of synthesis ($n = 10$). Radiochemical purity of the final product was >95%.

Data Acquisition

The animal's head was positioned in the ECAT EXACT HR+ PET scanner (Siemens/CTI, Knoxville, TN, USA) using a custom-designed stereotaxic head holder. A transmission scan was obtained to allow for attenuation correction. ^{11}C GSK189254 was then administered (134 \pm 50 MBq) intravenously as a bolus over 3 minutes and dynamic emission data were acquired for 2 hours (33 frames). Data were corrected for attenuation, randoms, scatter, and deadtime, and reconstructed using an attenuation-weighted OSEM algorithm.¹⁷

A structural T1-weighted magnetic resonance (MR) image of the baboon brain was also acquired to assist with anatomical localization of regions of interest. A T1-weighted coronal MR imaging sequence was used on a 3-T scanner (echo time (TE) = 3.34, repetition time (TR) = 2,530, 176 slices, slice thickness = 0.54 mm, flip angle = 7 degrees, image matrix = 256 \times 256, pixel size = 0.5 \times 0.5, field of view (FOV) = 140 mm, 3D turbo flash).

During each PET scan, 21 manual arterial blood samples were drawn to allow measurement of whole blood and plasma radioactivity and the parent fraction in plasma. In each scan, before injection of the radiotracer, a sample of fresh blood was collected to measure the radiotracer

plasma-free fraction (f_p) via ultrafiltration (Centrifree Micropartition Devices No. 4104 by Amicon, Dovers, MA, USA).

Analysis of the unchanged parent compound and its metabolites in arterial plasma samples collected at 6, 20, 40, 60, and 90 minutes after injection was performed by using a column-switching HPLC (high-performance liquid chromatography) assay.¹⁸ The parent compound retention time was around 13 minutes after injection. All the HPLC eluent was collected in fractions by an automated Spectrum Chromatography CF-1 fraction collection device. The counts of fractions were volume and decay corrected. The unmetabolized parent fraction was calculated as the ratio of the sum of radioactivity in the fractions containing the parent compound to the total amount of radioactivity collected. This fraction curve was also corrected for the time-varying extraction efficiency of radioactivity in corresponding filtered plasma samples. The fractions were then normalized to the recovery rate, which was determined by a reference plasma sample.

Additional arterial plasma samples were collected during scanning sessions 4 and 5 to assess the concentration of unlabeled GSK189254. Samples were collected at 5, 15, 30 minutes and 1, 2, 3, 5, 8, 14, 15, 17, and 18 hours postadministration of 1.5 μg /kg of unlabeled GSK189254 and stored at -80 °C for later analysis. Samples were analyzed by HPLC/MS/MS with a lower quantification limit of 20 pg/mL.

Data Analysis

Image analysis. Intermodality registration (MRI-to-PET) was performed using the automated image registration algorithm¹⁹ as an initialization step, followed by registration with NMI (normalized mutual information) to transform MRI into PET space. A baboon MRI template was also nonlinearly warped into the individual PET space via nonlinear registration (NMI-based linear plus nonlinear registration) to the subject's MRI. The template was created by averaging five individual baboon MRI images that were spatially normalized using an NMI-based linear plus nonlinear registration. Template regions for striatum, insula, and cerebellum, representing high, medium, and low uptake regions respectively, were applied to the dynamic PET data to generate regional TACs.

Input function. Arterial plasma activity samples were fitted to a model consisting of linear interpolation before the peak and a nonnegative sum of exponentials after the peak resulting in a continuous representation of the total arterial plasma activity. The parent fraction was fitted using a single exponential plus a constant model. The parent plasma input function was calculated as the product of the total arterial plasma curve and the fitted parent fraction curve. Whole blood samples were linearly interpolated to generate a continuous function. Due to technical difficulties, arterial blood samples were not collected for scan 2 in session 1. To avoid losing the scanning session, the data were analyzed using the baseline input function from the same scanning session, scaled for the difference in injected dose.

Estimation of in vivo affinity. The GSK189254 *in vivo* affinity was estimated using the methods presented in the Theory section (except the pseudoequilibrium method was excluded due to the lack of a reference region). For the MI method, the coinjection data obtained during the medium, high, and low SA sessions were used to obtain three independent estimates of K_d^{app} (one for each scanning session). Within a given scanning session, the implementation of the MI method consisted of fitting simultaneously the striatum, insula, and cerebellum, for baseline and coinjection scans, and constraining the value of k_{on} , k_{off} and the nondisplaceable volume of distribution V_{ND} to be the same across all regions. Therefore, for each MI scanning session (medium, high, and low SA) one estimate of K_d^{app} and three estimates of B_{avail} (striatum, insula, and cerebellum) were obtained.

The Direct PK-RO model was implemented in two different ways. First, equation 5 was used to relate V_T and the unlabeled GSK189254 plasma concentration; this method is referred to as 'Direct- V_T '. Regional V_T values were estimated using one- or two-tissue compartment models with the metabolite-corrected arterial input function. The appropriate tracer compartmental model was determined by the Akaike model selection criteria. For scanning sessions 1, 2, and 3, where the unlabeled plasma concentration of GSK189254 was not directly measured, plasma activity and SA measurements were used to estimate the unlabeled GSK189254 plasma concentration 1 hour after injection. Equation 5 was then fitted simultaneously to striatum, insula, and cerebellum V_T values as a function of the GSK189254 plasma concentration, constraining the value of V_{ND} and

K_d^{app} to be the same across all regions, with individual estimates of $BP_{ND}^{Baseline}$ for each region. Second, equation 3 was used to fit the TOC using the measured plasma concentration during scanning sessions 4 and 5 at 1, 6, and 15 hours after administration of 1.5 $\mu\text{g}/\text{kg}$ GSK189254; this method is referred to as 'Direct-TOC'. Here, the TOC at 1, 6, and 15 hours was estimated using the occupancy plot analysis²⁰ using average baseline V_T values (from sessions 1, 2, and 3) and the V_T values postdrug administration. Finally, the Indirect PK-RO model (equation 6) was applied to the TOC and plasma data, obtained from scanning sessions 4 and 5, to obtain a separate estimate of the affinity.

Simulations. Due to the impracticality of testing a large number of compounds with a broad range of kinetic properties, computer simulations were used to explore a wide range of compound kinetics and assess their impact on the estimation of affinity using both direct and indirect PK-RO models.

Using the nonlinear model equations (equations 1 and 2), a simulated set of TOCs was generated covering a range of parameter values (k_{off} : 1×10^{-4} to 0.02 min^{-1} , K_d : 0.01 to 0.4 nmol/L and k_2 : [0.01 0.1 1] min^{-1}). The measured arterial plasma time course of unlabeled GSK189254 obtained after the 1.5 $\mu\text{g}/\text{kg}$ dose (sessions 4 and 5) was used as the input function and k_{on} was reparameterized as $\frac{k_{off}}{K_d}$.

The TOC was defined as $C_5(t)/B_{avail}$ (for $t = 1, 6,$ and 15 hours) with B_{avail} arbitrarily fixed at 1 nmol/L. K_d was determined by fitting either the Direct or Indirect model to the simulated TOCs using the same GSK189254 input function. Differences in the estimated K_d from the true value were investigated as a function of k_{off} , K_d , and k_2 for both models. While k_{off} and K_d control the kinetics of the compound at the target site, k_2 was used to control the kinetics of the compound at the plasma-tissue interface. High values of k_2 (1 min^{-1}) resulted in rapid quasi-equilibrium between plasma and free tissue concentration (<15 minutes) while low values of k_2 (0.01 min^{-1}) produced much longer equilibration times (~ 30 hours). The simulated nondisplaceable volume of distribution V_{ND} ($=K_1/k_2$) was fixed to $1 \text{ mL}/\text{cm}^3$ to allow only k_2 to control the plasma-tissue dynamic.

The relationship between the Direct PK-RO model fit and the simulated target occupancy data was characterized by the goodness-of-fit (sum of squared error—SSE). The SSE was explored as a function of k_{off} , K_d , and k_2 for both models.

In the simulations described above, the duration of the study is defined as the time of the last simulated TOC sample (15 hours postdrug). To investigate the impact of study duration (T_d) on the estimates of k_{off} and K_d , a range of study durations were simulated ($T_d = 1$ to 24 hours) with two TOC samples (at $T_d/2$ and T_d hours) and these data were fit to the direct and indirect models.

RESULTS

All scans in the protocol were completed and no adverse events were observed due to the administration of GSK189254. An average of $7.0 \pm 0.2 \text{ ng}/\text{kg}$ of radioligand mass was injected during the tracer scans. Model fits obtained for scan 2 in session 1, where a scaled version of arterial blood activity was used, provided V_T estimates that were consistent with the rest of the data set.

The two-tissue compartment model with fixed blood volume ($V_b = 0.05$) was the most parsimonious model (as determined by the Akaike information criteria—AIC) for all regions and scans. The average plasma-free fraction was 0.62 ± 0.02 . Under the assumption of passive diffusion¹⁴ and using the average V_{ND} estimated from all the methods applied ($V_{ND} = 2.9 \pm 1.1 \text{ mL}/\text{cm}^3$), the estimated f_{ND} was 0.21. The average baseline V_T values ($n = 3$) for the striatum, insula, and cerebellum were 95 ± 8 , 67 ± 7 , and $40 \pm 2 \text{ mL}/\text{cm}^3$, respectively, which are consistent with previous reports in primates and humans.^{16,21}

A summary of target occupancy estimates derived from the slope of the occupancy plot are shown in Table 1.

Multiple Injection Method

The striatum, insula, and cerebellum were fitted simultaneously, generating individual estimates for B_{avail} and a single value for K_d^{app} . The coefficient of variation for K_d^{app} estimates decreased as the coinjection SA decreased (40%, 31%, and 24% for high,

Table 1. Target occupancy for all scanning sessions measured from the occupancy plots using the striatum, insula, and cerebellum

Scanning session	Occupancy (%)	Dose ($\mu\text{g}/\text{kg}$)	Time after administration (hours)
1	23	0.035	0 ^a
2	49	0.080	0 ^a
3	73	0.37	0 ^a
4	89	1.5	1
	81	1.5	6
5	54	1.5	15

^aCoinjection.

Table 2. Parameter estimates (equilibrium dissociation constant and available receptor density) obtained using the MI method ($\bar{x} \pm SE$) for striatum, insula, and cerebellum

Scanning session	K_d^{app} (nmol/L)	B_{avail} (nmol/L)		
		Striatum	Insula	Cerebellum
1	0.062 ± 0.025	5.3 ± 1.8	3.6 ± 1.0	2.0 ± 0.4
2	0.063 ± 0.019	4.1 ± 0.2	2.8 ± 0.1	1.6 ± 0.1
3	0.175 ± 0.043	6.8 ± 0.7	4.5 ± 0.4	2.6 ± 0.3
Average	0.100 ± 0.05	5.4 ± 2.0	3.7 ± 1.1	2.1 ± 0.5

MI, multiple injection. The asymptotic s.e.s were obtained from the parameter covariance matrix.

medium, and low SA) and this pattern was replicated for B_{avail} ($>20\%$ for high and between 10% and 5% for medium and low SA). The estimated V_{ND} for the three coinjection scanning sessions was $2.01 \pm 0.2 \text{ mL}/\text{cm}^3$.

Table 2 shows a summary of the coinjection parameter estimates obtained from the application of the MI method to scanning sessions 1, 2, and 3.

Direct- V_T PK-RO model

Figure 1 shows the fits of the direct PK-RO model to V_T using equation 5. The striatum, insula, and cerebellum data were fitted simultaneously with regional values of BP_{ND} for each region and common values for K_d^{app} and V_{ND} . The estimated K_d^{app} was $0.05 \pm 0.02 \text{ nmol}/\text{L}$, for B_{avail} ($=K_d^{app} BP_{ND}^{Baseline}/f_{ND}$) the values were $5.5 \pm 1.8 \text{ nmol}/\text{L}$, $3.6 \pm 1.3 \text{ nmol}/\text{L}$, and $2.0 \pm 0.9 \text{ nmol}/\text{L}$ for striatum, insula, and cerebellum, respectively, and V_{ND} was $4.4 \pm 5.2 \text{ mL}/\text{cm}^3$.

Indirect and Direct-Time Occupancy Curve PK-RO Model

The time course of the unlabeled GSK189254 plasma concentration obtained during scanning sessions 4 and 5 following the administration of 1.5 $\mu\text{g}/\text{kg}$ of unlabeled GSK189254 is shown in Figure 2A. The concentration peaks at ~ 5 minutes (1.8 nmol/L) with a terminal half-life of ~ 4 hours. Figure 2B shows the Indirect-TOC model fit (continuous line) to the target occupancy measurements at 1, 6, and 15 hours after administration of 1.5 $\mu\text{g}/\text{kg}$ unlabeled GSK189254. For comparison, the Direct-TOC model fit (dashed line) is also shown.

PK-RO model estimates of the GSK189254 affinity were $K_d^{app} = 0.073 \pm 0.018 \text{ nmol}/\text{L}$ (Direct $\bar{x} \pm SE$) and $K_d^{app} = 0.101 \pm 0.005 \text{ nmol}/\text{L}$ (Indirect $\bar{x} \pm SE$) where the standard errors (s.e.) were derived from the parameter covariance matrix obtained from the fitting procedure. Model selection criteria indicated that the Indirect model was preferred (AIC: -17 Direct versus -24 Indirect and F test $P = 0.05$).

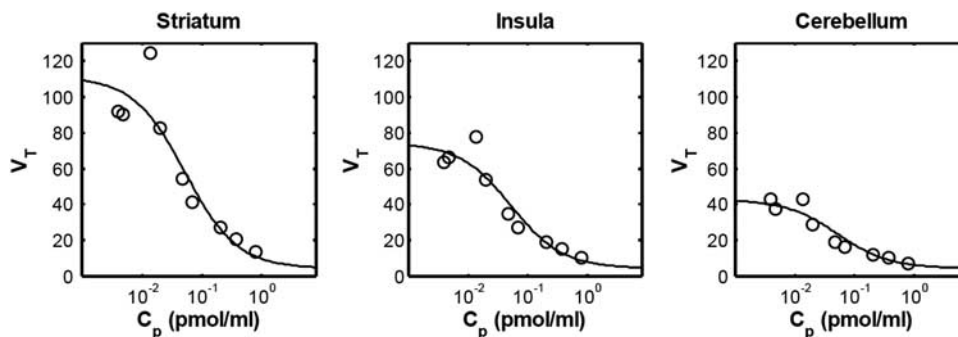


Figure 1. Direct model applied to three different brain regions. Open circles are the estimated V_T values. Solid line is the Direct PK-RO model fit. V_{ND} and K_d^{app} were constrained across the three regions.

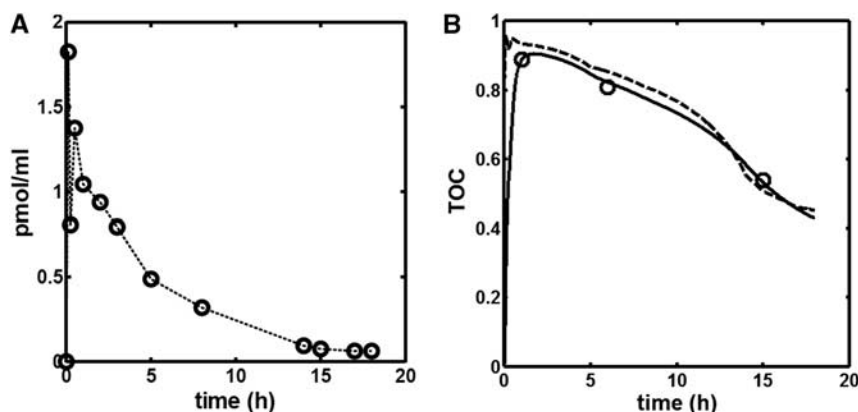


Figure 2. (A) Time course of unlabeled GSK189254 in plasma. (B) Direct and Indirect PK-RO model fits. Open circles are the measured H3 time occupancy curve (TOC) after administration of 1.5 µg/kg unlabeled GSK189254. Receptor occupancy at each time point was obtained from occupancy plots. Dashed and solid lines are the Direct (equation 3) and Indirect (equation 6) model fits respectively.

Table 3. Summary of GSK189254 K_d and K_d^{app} estimates obtained from four different analysis methods

		K_d^{app} (nmol/L)	K_d (nmol/L)
MI		0.100	0.021 ^a
Direct- V_T		0.052	0.032 ^b
PK-RO	Direct-TOC	0.073	0.045 ^b
	Indirect	0.101	0.063 ^b

MI, multiple injection; TOC, time occupancy curve. ^aCorrected for f_{ND} .
^bCorrected for f_p .

Table 3 shows a summary of the estimated equilibrium dissociation constants in the baboon across all different analysis methods.

Simulations

Figure 3A displays the SSE for the Direct PK-RO model as a function of K_d and k_{off} for a fixed value of $k_2 = 1 \text{ min}^{-1}$. As a general rule, the error for the Direct model was low when k_{off} values were high, that is, little lag between plasma and target bound concentrations, but this error became substantial as k_{off} becomes small, that is, substantial lag between plasma and target bound concentrations. The SSE obtained with the Indirect PK-RO model was consistently lower than that obtained with the Direct

model across the full K_d - k_{off} space, indicating that the Indirect PK-RO model always described the data better. In Figure 3B, the estimated error for K_d with the Direct model is shown as a function of K_d and k_{off} . The low-error region with k_{off} values smaller than 0.005 min^{-1} (dark stripe in the lower part of the figure) corresponds to an artifact where the K_d is estimated correctly whilst the model fit is poor.

Slower rates of equilibration between plasma and tissue, as simulated by decreasing values of k_2 , showed a similar pattern to those shown in Figure 3A with a worsening of the Direct PK-RO representation of the data accompanied by a poorer estimation of K_d . For example, when the simulated K_d and k_{off} were identical to the ones estimated from the GSK189254 *in vivo* study, the direct model SSE increased ~ 3 -fold for $k_2 = 0.1$ and ~ 53 -fold for $k_2 = 0.01$ as compared with $k_2 = 1$. Figure 3C shows four examples of the Direct and Indirect model fits to the simulated data. Each plot corresponds to points depicted in Figures 3A and 3B. The GSK189254 plot was obtained using the k_{off} and K_d estimates obtained from the *in vivo* GSK189254 experiment. In (i) the value of k_{off} is fourfold smaller than in the GSK189254 plot. In (ii) K_d is fourfold larger than in the GSK189254 plot. Plot (iii) is an example where the Direct model correctly estimates K_d but the model fit is poor. In all these examples, the Indirect PK-RO model accurately estimates the K_d .

Figure 4 shows the effect of the study duration (T_d) on K_d %bias for the direct and indirect models for three different values of k_{off} (0.001, 0.005, and 0.01 min^{-1} in A, B, and C, respectively). The values for k_2 and K_d were fixed at 1 min^{-1} and 0.06 nmol/L , respectively. In general, for the indirect model, the smaller the

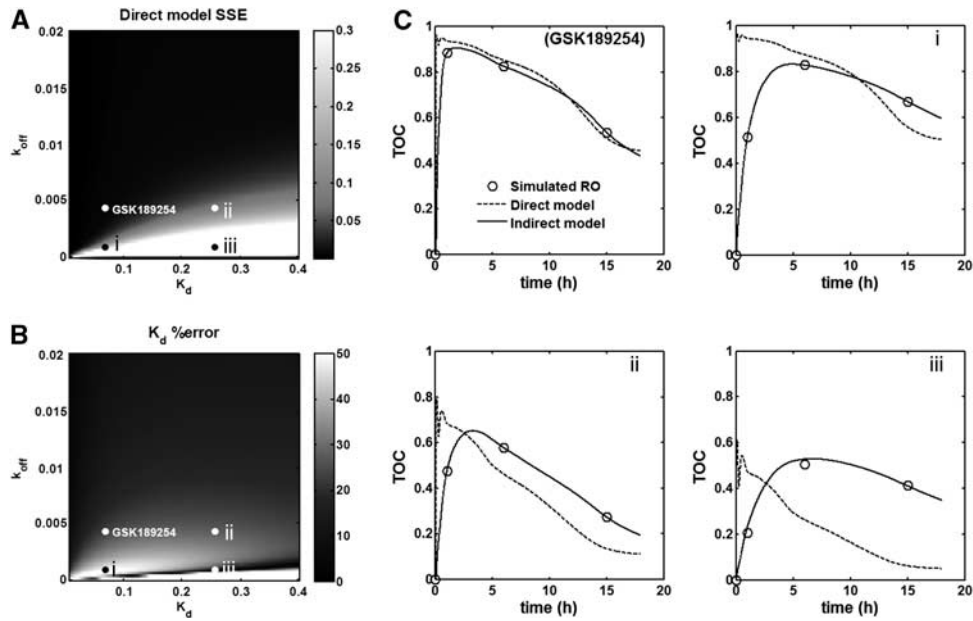


Figure 3. (A) SSE (sum of square errors) between the Direct PK-RO model fit and the simulated time occupancy curve (TOC). Brighter regions represent a larger error while darker areas represent smaller errors. (B) Error between the true K_d and the Direct PK-RO estimate of K_d expressed as the absolute value in percentage. (C) Four examples of Direct (dashed) and Indirect (solid) model fits corresponding to the points depicted in (A) and (B). The upper left plot represents simulated data using the parameters estimated for GSK189254 from the *in vivo* experiments. Plots i, ii and iii present clear examples of pharmacological hysteresis.

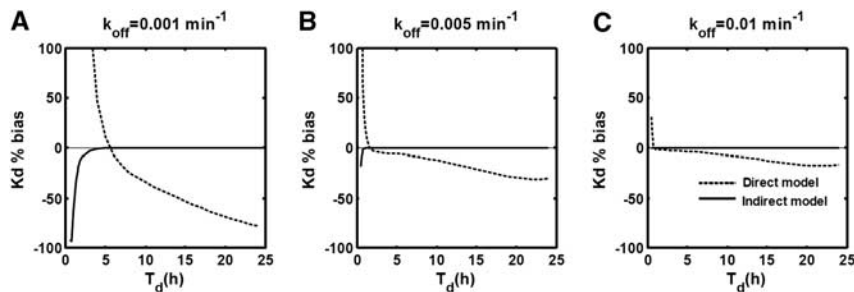


Figure 4. Effect of the study duration (T_d) on the accuracy of direct (dashed line) and indirect (solid line) estimates K_d for three different values of k_{off} : (A) 0.001 min^{-1} , (B) 0.005 min^{-1} , and (C) 0.01 min^{-1} .

value of k_{off} (increased lag between plasma and target bound concentrations) the longer the time needed to accurately estimate the true simulated K_d (e.g., ~ 5 hours for $k_{off} = 0.001 \text{ min}^{-1}$ and only ~ 1 hour when $k_{off} = 0.01 \text{ min}^{-1}$). In contrast, with the exception of coincidental cases similar to those observed in Figure 3, the direct model always produced biased estimates of K_d independent of the study duration.

DISCUSSION

Estimation of the *in vivo* affinity of compounds has an important role in the development of novel drugs that bind reversibly to specific molecular targets in the brain. For example, an accurate estimation of *in vivo* affinity from early first time in human studies, in conjunction with knowledge of the desired target occupancy, facilitates optimal dose selection for larger clinical trials. In the PET field, accurate measurement of the *in vivo* affinity can also be important in providing confidence that mass dose effects are not present.

Positron emission tomography methods for the estimation of *in vivo* affinity can be grouped into two categories: (1) those applicable only to homologous competition studies and (2) those applicable to both homologous and heterologous competition studies. When the compound of interest is itself radiolabeled with

a PET isotope and possesses a quantifiable specific signal, homologous competition studies can be performed and analyzed to estimate the affinity of the compound. However, more usually, the labeled compound does not possess suitable characteristics to allow quantification of the specific signal. In these cases, one must rely on an established PET radioligand that binds to the same target as the compound of interest and measure changes in the PET signal due to heterologous competitive binding between the radioligand and the unlabeled compound of interest. These data can then be analyzed by direct or indirect PK-RO methods described here. In addition, these PK-RO methods can be applied to homologous competition studies (as has been done here with GSK189254 as part of this investigative work).

All these methods, whether applied to homologous or heterologous competition, characterize the pharmacokinetic relationship between plasma (or a surrogate measurement of free tissue concentration in the case of the transient equilibrium method) and target bound concentrations of the unlabeled compound of interest to estimate its *in vivo* affinity. However, each method makes different assumptions about the rate of exchange between different compartments in its transit between plasma and the target and vice versa. Consequently, it is possible to obtain incorrect estimates of the *in vivo* affinity if the assumptions made by the model are invalid. In particular, if the compound

displays pharmacological hysteresis and the model does not allow for a dynamic lag between plasma and target bound concentrations then the affinity estimates will be invalid. For example, the MI method treats the BBB transit and the binding process separately. When the injection protocol is appropriately optimized,^{6,22} these two processes can be isolated making it possible to estimate the affinity of the compound. On the other hand, with the pseudoequilibrium method, although the relationship between the surrogate bound concentration (obtained by subtracting the target and the reference TACs) and the free tissue concentration arises from an equilibrium condition, differences between the true and surrogate bound concentrations can lead to errors in the estimated affinity. The application of the direct PK-RO method to heterologous competition assumes that the plasma and bound concentration are in instantaneous equilibrium at all times and ignores any finite exchange processes in BBB transport and target binding. The indirect PK-RO model tries to address these limitations by introducing a finite exchange process for the target binding while the BBB transit is assumed to equilibrate instantaneously. Although a more comprehensive heterologous method could be defined along the lines of the MI model that accounts for both BBB transit and target binding, the limited data obtained during a heterologous type of study (usually two or three occupancy time points) would make it difficult to kinetically separate BBB transit and target binding.

In our hands, the four different analysis methods produced similar subnanomolar affinity estimates of GSK189254 in the baboon study (Table 3). Model selection criteria did indicate a preference for the Indirect over the Direct PK-RO model; however, the difference in Akaike score was modest and the F test indicated only a borderline improvement. These results suggest that the dynamic lag between plasma and target bound concentrations of GSK189254 was small in baboon and that the application of models that do not account for pharmacological hysteresis are relatively unbiased.

Computer simulation allowed us to explore scenarios where there was an increased dynamic lag between plasma and target bound concentrations to investigate the impact on K_d estimation. The equilibration rate between plasma and tissue across the BBB, which is not explicitly considered in the Indirect PK-RO model, was modified via k_2 with smaller values producing longer equilibration times, whilst the equilibration rate between tissue and target was modified via k_{off} and K_d . Figure 3A and 3B show the performance of the Direct PK-RO model when k_2 is fixed (1 min^{-1}). As expected, for smaller k_{off} or larger K_d values, which increase the dynamic lag between plasma and target bound concentrations, there was an increasingly poor prediction of the target occupancy (Figure 3A). The pattern observed in Figure 3B showed a region of small differences between the estimated and the true K_d (dark area below values of 0.005 min^{-1} for k_{off}) that represents an artifact for cases in which the equilibrium dissociation constant is correctly predicted in spite of significant data-model mismatch.

For the Indirect PK-RO model, when plasma and free tissue concentrations could be considered in equilibrium at all times ($k_2 = 1$), the model always described the simulated TOC correctly (small SSE values) regardless of the simulated value of k_{off} or K_d and consequently the K_d was accurately estimated ($\text{mean}(|K_d \% \text{bias}|) \sim 1\%$) except when the simulated k_{off} value approached 0. The simulations also showed that when there was little dynamic lag between plasma and target bound concentrations (represented by increasing values of k_{off}) the estimation of k_{off} becomes inaccurate, suggesting that the processes of dissociation from the target and tissue clearance cannot be identified by the indirect model when they are kinetically similar or when the plasma clearance is the limiting factor.

Examples in Figure 3C show that the Indirect PK-RO model always described the TOCs correctly even when a substantial lag exists between plasma and target bound concentrations, while

the direct PK-RO model fails when k_{off} is small and/or when K_d is high. The rate of equilibration between plasma and tissue (effect of k_2) was also investigated for the indirect PK-RO model. Slower rates of equilibration between plasma and tissue ($k_2 = 0.1$ and 0.01 min^{-1}) had a small impact on the K_d estimates with an average bias of $\sim 10\%$ for the smallest value of k_2 . However, a substantial impact on the accuracy of the k_{off} estimates was observed when the equilibration between plasma and tissue was slow (from $\sim 10\%$ for $k_2 = 1 \text{ min}^{-1}$ increasing to $\sim 80\%$ for $k_2 = 0.01 \text{ min}^{-1}$).

Simulations investigating the impact of study duration (T_d) on the accuracy of K_d estimates revealed that the indirect model was able to accurately recover the K_d unless the kinetics of the compound were particularly slow or T_d was too short such that the TOC appeared irreversible with respect to the plasma concentration. It should be noted that the choice of doses and times at which the TOC is sampled has an impact on the precision of the affinity estimates²³ but that this should not change these general findings. In contrast, the direct model repeatedly failed to recover the true K_d value (except for artifactual cases explained previously). Exploration of these data indicated that the direct model underestimates the value of K_d by a factor that depends on the terminal washout of the free concentration ($K_d^{\text{direct}} = (k_{off} - \beta)/k_{on}$) where β is the terminal washout rate of the free concentration. This is analogous to errors introduced in the quantification of a PET partition coefficient (V_T) from the ratio of nonequilibrium tracer data.²⁴

In summary, noise-free computer simulations have demonstrated that the indirect PK-RO model is a robust approach for the estimation of K_d even under conditions of pharmacological hysteresis. When the drug-target interaction is the rate-limiting process, k_{off} can also be estimated. It is beyond the scope of this work to investigate the effects of noise in the plasma and occupancy measurements on the estimation of the model parameters; however, it is recognized that for the data presented, the indirect model estimates two parameters from three data points and as such the estimates have the potential to be sensitive to noise.

CONCLUSION

Positron emission tomography can achieve characterization of the *in vivo* pharmacokinetic properties of compounds that reversibly bind to molecular targets in the brain. Although the selection of the appropriate analysis method depends on study design factors (e.g., homologous versus heterologous competition and the presence or absence of a reference region), it is also important to consider the kinetics of the compound under investigation and select an appropriate biological model that may need to account for pharmacological hysteresis.

DISCLOSURE/CONFLICT OF INTEREST

The authors declare no conflict of interest.

ACKNOWLEDGEMENTS

The authors acknowledge the expert assistance of Krista Fowles, Shervin Liddie, Siobhan Ford, Christine Sandiego and the rest of the team at the Yale PET Center.

REFERENCES

- 1 Campbell DB. The use of kinetic-dynamic interactions in the evaluation of drugs. *Psychopharmacology (Berl)* 1990; **100**: 433–450.
- 2 Slifstein M, Laruelle M. Models and methods for derivation of *in vivo* neuroreceptor parameters with PET and SPECT reversible radiotracers. *Nucl Med Biol* 2001; **28**: 595–608.

- 3 Delforge J, Janier M, Syrota A, Crouzel C, Vallois JM, Cayla J *et al*. Noninvasive quantification of muscarinic receptors *in vivo* with positron emission tomography in the dog heart. *Circulation* 1990; **82**: 1494–1504.
- 4 Morris ED, Babich JW, Alpert NM, Bonab AA, Livni E, Weise S *et al*. Quantification of dopamine transporter density in monkeys by dynamic PET imaging of multiple injections of ¹¹C-CFT. *Synapse* 1996; **24**: 262–272.
- 5 Christian BT, Narayanan T, Shi B, Morris ED, Mantil J, Mukherjee J. Measuring the *in vivo* binding parameters of [¹⁸F]-fallypride in monkeys using a PET multiple-injection protocol. *J Cereb Blood Flow Metab* 2004; **24**: 309–322.
- 6 Salinas C, Muzic Jr RF, Ernsberger P, Saidel GM. Robust experiment design for estimating myocardial beta adrenergic receptor concentration using PET. *Med Phys* 2007; **34**: 151–165.
- 7 Farde L, Eriksson L, Blomquist G, Halldin C. Kinetic analysis of central [¹¹C]raclopride binding to D₂-dopamine receptors studied by PET—a comparison to the equilibrium analysis. *J Cereb Blood Flow Metab* 1989; **9**: 696–708.
- 8 Holden JE, Jivan S, Ruth TJ, Doudet DJ. *In vivo* receptor assay with multiple ligand concentrations: an equilibrium approach. *J Cereb Blood Flow Metab* 2002; **22**: 1132–1141.
- 9 Zhang L, Beal SL, Sheiner LB. Simultaneous versus sequential analysis for population PK/PD data I: best-case performance. *J Pharmacokinet Pharmacodyn* 2003; **30**: 387–404.
- 10 Abanades S, van der Aart J, Barletta JA, Marzano C, Searle GE, Salinas CA *et al*. Prediction of repeat-dose occupancy from single-dose data: characterisation of the relationship between plasma pharmacokinetics and brain target occupancy. *J Cereb Blood Flow Metab* 2011; **31**: 944–952.
- 11 Ariens EJ. Molecular basis of drug action. *Med Arh* 1964; **18**: 21–38.
- 12 Derendorf H, Meibohm B. Modeling of pharmacokinetic/pharmacodynamic (PK/PD) relationships: concepts and perspectives. *Pharm Res* 1999; **16**: 176–185.
- 13 Medhurst AD, Atkins AR, Beresford IJ, Brackenborough K, Briggs MA, Calver AR *et al*. GSK189254, a novel H₃ receptor antagonist that binds to histamine H₃ receptors in Alzheimer's disease brain and improves cognitive performance in preclinical models. *J Pharmacol Exp Ther* 2007; **321**: 1032–1045.
- 14 Innis RB, Cunningham VJ, Delforge J, Fujita M, Gjedde A, Gunn RN *et al*. Consensus nomenclature for *in vivo* imaging of reversibly binding radioligands. *J Cereb Blood Flow Metab* 2007; **27**: 1533–1539.
- 15 Csajka C, Verotta D. Pharmacokinetic-pharmacodynamic modelling: history and perspectives. *J Pharmacokinet Pharmacodyn* 2006; **33**: 227–279.
- 16 Ashworth S, Rabiner EA, Gunn RN, Plisson C, Wilson AA, Comley RA *et al*. Evaluation of ¹¹C-GSK189254 as a novel radioligand for the H₃ receptor in humans using PET. *J Nucl Med* 2010; **51**: 1021–1029.
- 17 Comtat C, Kinahan P, Défrise M, Michel C, Townsend D. Fast reconstruction of 3D PET data with accurate statistical modeling. *IEEE Trans Nucl Sci* 1998; **45**: 1083–1089.
- 18 Hilton J, Yokoi F, Dannals RF, Ravert HT, Szabo Z, Wong DF. Column-switching HPLC for the analysis of plasma in PET imaging studies. *Nucl Med Biol* 2000; **27**: 627–630.
- 19 Woods RP, Mazziotta JC, Cherry SR. MRI-PET registration with automated algorithm. *J Comput Assist Tomogr* 1993; **17**: 536–546.
- 20 Cunningham VJ, Rabiner EA, Slifstein M, Laruelle M, Gunn RN. Measuring drug occupancy in the absence of a reference region: the Lassen plot re-visited. *J Cereb Blood Flow Metab* 2010; **30**: 46–50.
- 21 Logan J, Carruthers NI, Letavic MA, Sands S, Jiang X, Shea C *et al*. Blockade of the brain histamine H₃ receptor by JNJ-39220675: preclinical PET studies with [(11)C]GSK189254 in anesthetized baboon. *Psychopharmacology (Berl)* 2012; **223**: 447–455.
- 22 Delforge J, Syrota A, Mazoyer BM. Experimental design optimisation: theory and application to estimation of receptor model parameters using dynamic positron emission tomography. *Phys Med Biol* 1989; **34**: 419–435.
- 23 Zamuner S, Di Iorio VL, Nyberg J, Gunn RN, Cunningham VJ, Gomeni R *et al*. Adaptive-optimal design in PET occupancy studies. *Clin Pharmacol Ther* 2010; **87**: 563–571.
- 24 Carson RE, Channing MA, Blasberg RG, Dunn BB, Cohen RM, Rice KC *et al*. Comparison of bolus and infusion methods for receptor quantitation: application to [¹⁸F]cyclofoxy and positron emission tomography. *J Cereb Blood Flow Metab* 1993; **13**: 24–42.